International Research Journal of Innovations in Engineering and Technology (IRJIET)

ISSN (online): 2581-3048
Volume 7, Issue 5, pp 154-159, May-2023
https://doi.org/10.47001/IRJIET/2023.705017

Flow Analysis of Pertamina-Dex in Curved Pipe Line at the Integrated Terminal of Pertamina Patra Niaga Semarang

[1]Sefrian Imam B, [2]*Khoiri Rozi, [3]Agus Suprihanto, [4]Susilo Adi W, [5]Yunianto Arif S

[1,2,3,4]Mechanical Engineering, Diponegoro University, Semarang, Indonesia
Jl. Prof. H. Soedarto, SH, Tembalang, Semarang 50275
[5]PT Pertamina Patra Niaga Integrated Terminal Semarang, Semarang, Indonesia
Jl. Pengapon, Kemijen, Kota Semarang 50227
*Corresponding Author E-mail: khoiri.rozi@yahoo.com

Abstract **- This research was carried out to understand the flow characteristics of Pertamina Dex through the elbow in pipe line systems. The work was made using ANSYS FLUENT with the *k-εRNG* turbulence model. The results of the Pertamina-Dex flow simulation at the elbow with Re = 165.748 produce a maximum speed of 1.24522 m/s, with a pressure drop of 1471 Pa, and a maximum temperature of 301.392K. While the results of the flow simulation with Re = 350.551 produce a maximum speed of 2.6088 m/s, with a pressure drop of 5439 Pa, and a maximum temperature of 300.709K.**

Keywords: Curved Pipe, Secondary Flow, Pressure Loss, Turbulent Flow.

I. INTRODUCTION

Elbow is an arch-shaped channel that is often found in piping system networks in the oil industry [3]. Elbow makes it easy to change the direction of oil flow but can cause flow instability and pipe friction [11]. Elbow causes a change in direction which can result in flow stability due to centrifugal force. When flow enters the elbow, the velocity and flow characteristics are difficult to understand. In the horizontal elbow which is affected by centrifugal force, and in the vertical elbows which is affected by gravity. Centrifugal force creates a flow phenomenon called secondary flow. This type of flow can cause pressure drops and losses. The higher the flow velocity when it enters the elbow, the higher the centrifugal force so that the pressure drop increases [5].

The pressure drop in the elbow is not only caused by the centrifugal force of the flow but also caused by the friction of the fluid with the pipe wall. The type of fluid and pipe material also greatly affect the pressure drop, because the higher the viscosity of the fluid and the roughness of the pipe material, the greater the resulting frictional force so that the pressure drop increases [5].

Research on the flow regime at the elbow especially to study flow phenomena such as characterization and heat transfer using Newtonian fluids has become a broad topic, both experimentally and numerically. The subject for laminar flow and involving convective heat transfer for a 180° elbow have been reviewed by Arvanitis et al. [1] by analyzing non dimensional parameters including Nusselt numbers, Reynolds numbers, Prandtl numbers, and Dean numbers. Ayala and Cimbala [2] examined the phenomenon of turbulent flow at the elbow by comparing several existing turbulent models and the results said that the k-ε turbulence models produced the most accurate results. Rawat et al. [8] have analyzed the performance of an elbow meter for high concentration coal ash slurry which behaves as a homogeneous liquid with behavior as a Bingham plastic liquid. They relate the elbow meter coefficient to the Reynolds number, radius ratio, pipe roughness, and storm number. They also analyzed the pressure drop that occurs on the number of mesh elements and speed variations using variations of the turbulent model.

Numerically, Ikarashi et al. [4] investigated turbulent flow at 90^o elbow with a radius ratio of 1.0-1.5 and Reynolds number Re = 3×10^4 – 10×10^4. They compared the distribution of velocity, axial turbulence intensity, and Reynolds stress to the ratio of height to diameter (y/D) and also analyze the secondary flow to the variation of Reynolds number. Sutton et al. [10] analyzed the dynamic characteristics and pressure losses of viscous-plastic and elastoviscous-plastic flows through 90^o pipe bends. They succeeded in predicting the pressure loss of the viscous-plastic fluid flow at the elbow which was accurate to within 1% at Regen to 10.

This study was made in order to get a detailed description regarding the characteristics of flow through the elbow arrangement in the piping system at Pertamina Patra Niaga Integrated Terminal Semarang. Simulations were made using

International Research Journal of Innovations in Engineering and Technology (IRJIET)

ISSN (online): 2581-3048

Volume 7, Issue 5, pp 154-159, May-2023

https://doi.org/10.47001/IRJIET/2023.705017

ANSYS Fluent Software with two elbow models and two variations of the Reynolds number.

II. METHODOLOGY

2.1 Model and Geometry

The basic geometry of the pipe was made using the software of Solid-works 2020. The pipe model was made according to the conditions at Patra Niaga Integrated Terminal Semarang. This pipe has a diameter dimension of 16" SCH 40. Detailed modeling sizes can be seen in Figure 1 and Table 1. This simulation was carried out using the 3D Model ANSYS fluent 2020R2. The pipe used is API 5L Grade B SCH 40 with a size of 16 "with carbon steel material. The pipe physical properties were obtained from the experimental results of Rosman and Pao [7], which can be seen in Table 2.

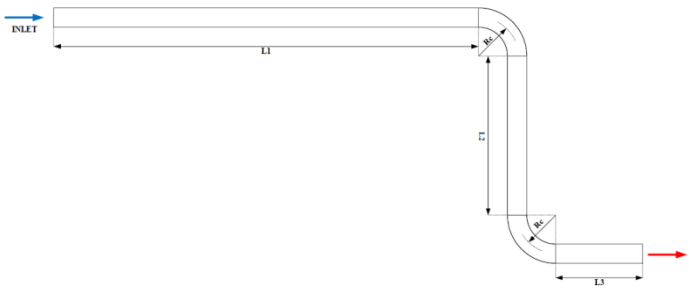

Figure 1: Pipe Geometry of two-dimensional (2D) Model

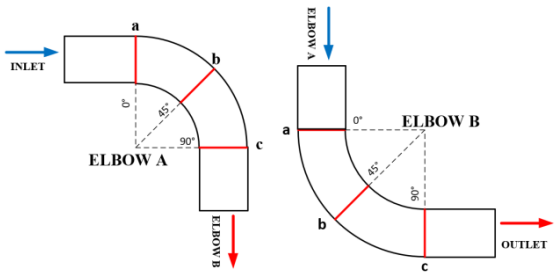

Figure 2: Detail simulation locations

Table 1: Detail model parameters

Parameter	Value	Units
L1	60	m
L2	41	m
L3	8.5	m
Rc	0.457	m
ID	0.397	m
OD	0.406	m

Table 2: Pipe Properties

Property	Symbol	Value	Units
Density	ρ	7850	kg/m^3
Thermal Conductivity	k	54	W/(m.K)
Specific Heat Capacity	C_p	502,4	J/(kg.K)
Heat Flux	q"	900	W/m^{2}K

2.2 Mesh Generation

The mesh shape used in this simulation is polyhedral with an average skewness = 0.038 and a minimum orthogonal quality > 0.2001. In order to capture the physical phenomena at the boundary layer between the fluid and the wall, an inflation layer is created. Based on the independent grid test results, the number of mesh cells is 2,010,625. The mesh structure is shown in Fig. 3 below.

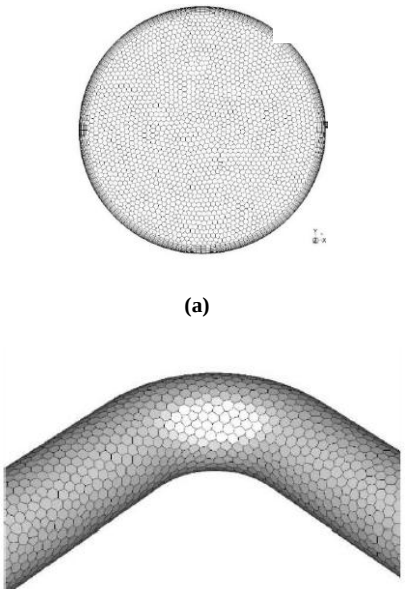

(a)

(b)

Figure 3: Mesh Structure (a) Cross section of Elbow (b) Elbow model

2.3 Boundary Condition

In this simulation, the boundary conditions used in the model are fixed domain, velocity inlet, energy on and pressure outlet. Details of the boundary conditions in this study can be seen in Table 3 below.

Table 3: Set-Up Models

Inlet	Velocity	0,835 1,766 (m/s)
	Temperature	300^{o}K
Outlet	Gauge Pressure	300.000 Pa
Wall	Heat Flux	900 W/m^{2}K
Residual		9e10^{-5}

The fluid used in this research is liquid Pertamina-Dex. Thermal Conductivity (k) and Specific Heat (Cp) data were taken from Lin and Ronghong [5]. The speed used in the inlet is taken from two ships namely, Gandawati Ship and Total Energy Ship with speeds of 0.835 m/s and 1.766 m/s. The inflow is made long with the aim that the turbulent flow is fully developed [6]. Detailed physical properties are summarized in Table 4 below.

International Research Journal of Innovations in Engineering and Technology (IRJIET)

ISSN (online): 2581-3048

Volume 7, Issue 5, pp 154-159, May-2023

https://doi.org/10.47001/IRJIET/2023.705017

Table 3: Pertamina-Dex properties

Property	Symbol	Value	Units
Density	ρ	811	kg/m^3
Thermal Conductivity	k	1,39	W/(m.K)
Specific Heat Capacity	C_p	1900	J/(kg.K)
Dynamic Viscosity	μ	1662	$\mu Pa * s$

2.4 Turbulence Model

The turbulent model used in this study is the k-ε RNG. According to Ayala and Cimbala [2] this turbulent model produces simulations in the elbow with the highest accuracy. The K-ε RNG model equation for turbulent flow is derived from the Navier-Stokes equation as follows:

$$\frac{\partial}{\partial t}(\rho k) + \frac{\partial}{\partial x_i}(\rho k u_i) = \frac{\partial}{\partial x_j}\left[\alpha_k \mu_{eff} \frac{\partial k}{\partial x_j}\right] + G_k + G_b - \rho\epsilon - Y_M + S_k \quad (1)$$

Dan

$$\frac{\partial}{\partial t}(\rho\epsilon) + \frac{\partial}{\partial x_i}(\rho\epsilon u_i) = \frac{\partial}{\partial x_j}\left[\alpha_\epsilon \mu_{eff} \frac{\partial \epsilon}{\partial x_j}\right] + C_{1\epsilon}\frac{\epsilon}{k}(G_k + GbC3\epsilon - C2\epsilon\rho\epsilon 2k - R\epsilon + S\epsilon \quad (2)$$

where, G_k is the turbulence kinetic energy generated due to the average velocity gradient, G_b is the turbulence kinetic energy generated due to buoyancy, Y_M is the dilatation that fluctuates in compressible turbulence with respect to the overall dissipation rate, $C_{1\epsilon}$, $C_{2\epsilon}$, and $C_{3\epsilon}$ are constants, αk and αϵ are Inverse effective Prandtl numbers for k and ε, and Sϵ are additional sources determined by the author.

With the scale elimination procedure, the RNG differential equation for turbulent viscosity is produced, namely:

$$d\left(\frac{\rho^2 k}{\sqrt{\epsilon\mu}}\right) = 1{,}72\frac{\hat{v}}{\sqrt{\hat{v}^3 - 1 + C_v}} d\hat{v} \quad (3)$$

Where:

$$\hat{v} = \frac{\mu_{eff}}{\mu}, C_v \approx 100 \quad (4)$$

Within the limits of the high Reynolds number, then

$$\mu_t = \rho C_\mu \frac{k^2}{\epsilon}, \text{dengan nilai} C_\mu = 0{,}0845 \approx 0{,}09 \quad (5)$$

III. RESULTS AND DISCUSSIONS

3.1 Flow structure

The results of secondary flow simulation and velocity distribution on the two elbows A and B with Reynolds numbers Re = 165,748 and 350,551 can be seen in Figures 4 and 5. The plot arrangement is sorted according to Figure 2 from top to bottom, angles θ = 0°, 45° and 90°. Velocity is represented by color degradation on the right side of the plot where low speed is represented in blue and high speed is represented in red. The flow velocity reaches a maximum on the inner surface of the elbow and at an angle of 45o. From the two plots for the two elbows, it can be seen that the structure of the secondary flow at each corner position is almost the same. At the 0o angle position it can be seen that the secondary flow has not been formed then when it enters the 45o angle position the secondary flow looks very strong and after that it will experience a decrease with the center of the vortex shifting to the inner diameter of the elbow when it exits the elbow (90°) for both elbows and both Re tested.

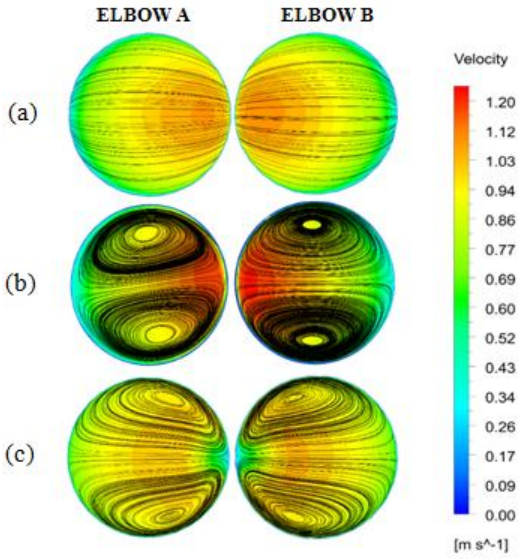

Figure 4: Secondary Flow with Velocity Contours at Re = 165.748 in the three locations of Elbow A and B for (a) θ = 0°,(b) θ= 45°, and (c) θ= 90°

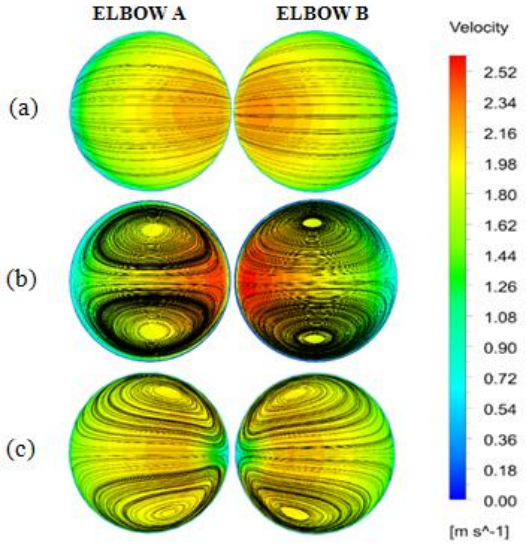

Figure 5: Secondary Flow with Velocity Contours at Re = 350.551 in the three locations of Elbow A and B for (a) θ = 0°, (b) θ =45°, and (c) θ = 90°

International Research Journal of Innovations in Engineering and Technology (IRJIET)

ISSN (online): 2581-3048

Volume 7, Issue 5, pp 154-159, May-2023

https://doi.org/10.47001/IRJIET/2023.705017

3.2 Velocity Profile

Figures 6(a-b) and 7(a-b) are velocity profiles of the simulation results on two elbows A and B with variations in Reynolds number Re = 165,748 and 350,551. Velocity profiles are taken in horizontal and vertical positions along the pipe diameter of both elbows. The speed profile is used to show the location of the maximum and minimum speed values at the elbow. From the plots of the two elbows tested it was found that for Re = 165,748 it has a maximum speed u = 1.245 m/s and a minimum u = 0 m/s, while for Re = 350,551 it has a maximum speed u = 2.608 m/s and a minimum u = 0 m /s. From the vertical velocity profile plot for the two variations of the Reynolds number the two elbows have almost the same shape with the maximum speed value being at the point r/R = 0.0. Meanwhile, from the horizontal velocity profile plot, it is found that the maximum speed for locations a and b is at r/R = 0.8 while at locations at r/R = 0.4 for both Reynolds numbers tested as shown in the plot.

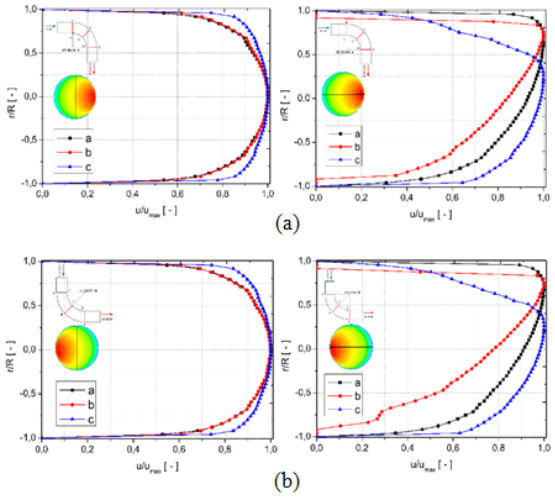

Figure 6: Normalized Velocity Profile at Re = 165.748 for (a) Elbow A and (b) Elbow B

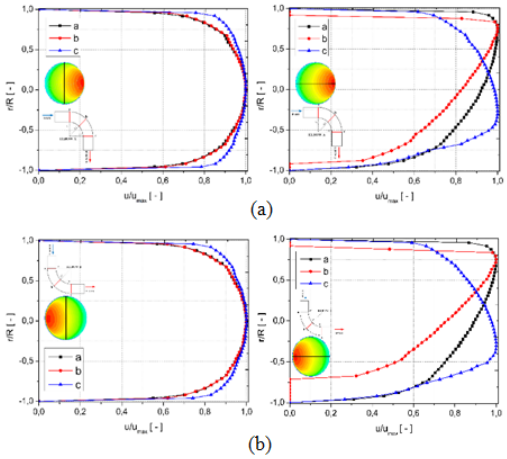

Figure 7: Normalized Velocity Profile at Re = 350.551for (a) Elbow A and (b) Elbow B

At elbows A and B for positions 0°, and 45° have a similar shape in both variations of the Reynolds number, where the velocity profile is more inclined to the part near the inner wall of the elbow with maximum speed at the point r/R = 0.8, whereas in the elbow position 90° the velocity profile for the two variations of the Reynolds number has a different shape with Re = 165,748 the velocity profile has a maximum value at point r/R = 0.3 while at Re = 350,551 at point r/R = -0.3. This happens because there is a difference in speed so that the resulting profile due to different elbows.

3.3 Pressure Loss

The flow pressure profile graphs at both elbows A and B for the simulation results for Re = 165.748 and 350.551 are plotted in Figures 8(a-b) and 9(a-b). From the graph it can be seen that the pressure value before entering the elbow is greater than after leaving the elbow. The maximum pressure at Re = 165,748 is 301,471 Pa and the minimum pressure is 299,693 Pa. Meanwhile, from the plot for Re = 350,551 it is found that the maximum pressure is 305,439 Pa and the minimum pressure is 298,541 Pa. The pressure profiles at the two elbows with two variations of the Reynolds number have a similar shape. In the vertical conditions for both elbows for position 0° the pressure profile is high near the wall and drops in the middle of the pipe, while for positions 45° and 90° the pressure profile is high near the wall and decreases at the point r/R = 0.7-0.85 then increases again in the middle of the pipe.

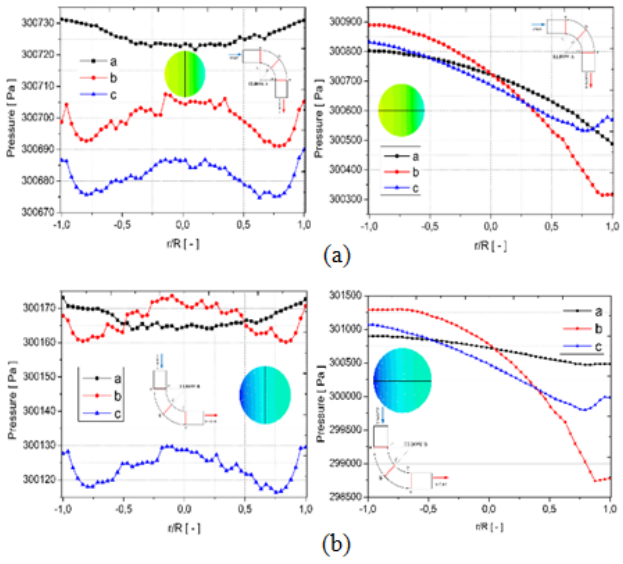

Figure 8: Pressure distribution at Re = 165.747,5 for (a) Elbow A and (b) Elbow B

In the horizontal conditions for both elbows, they experience a rather monotonous change where the pressure decreases continuously near the inner wall of the elbows at the three simulated locations. The maximum pressure is located at the inlet and the minimum at the outlet, so that the flow with

International Research Journal of Innovations in Engineering and Technology (IRJIET)

ISSN (online): 2581-3048

Volume 7, Issue 5, pp 154-159, May-2023

https://doi.org/10.47001/IRJIET/2023.705017

Re = 165,748 experiences a pressure loss of 1471 Pa and the test with Re = 350,551 experiences a pressure loss of 5439 Pa.

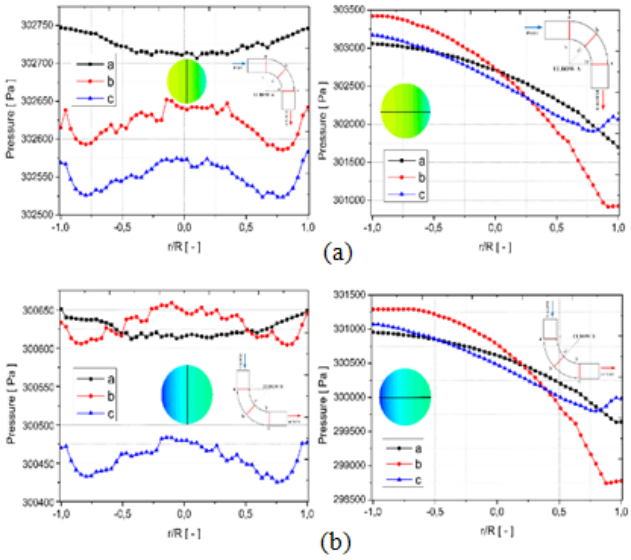

Figure 9: Pressure distribution at Re = 350.551for (a) Elbow A and (b) Elbow B

3.4 Temperature

The simulation results of the temperature distribution on the two elbows A and B with both variations of the Reynolds number Re = 165.7748 and 350.551 are presented in Figures 10(a-b) and 11(a-b). From the graph above, it can be seen that the greater the Reynolds number, the smaller the friction factor so that the heat transfer increases, as a result the temperature value becomes smaller. The temperature values for Re = 165.748 and 301.392 K and a minimum of 300 K, while for Re = 350.551 it has a maximum temperature of 300.709 K and a minimum of 300 K.

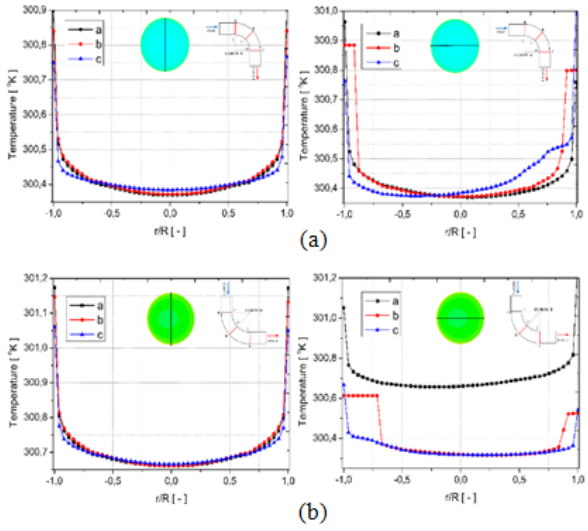

Figure 10: Temperature distribution at Re = 165.747,5 for (a) Elbow A and (b) Elbow B

The flow in the pipe has a temperature difference caused by the frictional force on the wall. The highest temperature is in the area near the pipe wall for all conditions tested. In general, the further away from the wall the temperature value decreases, so that the smallest temperature value is in the middle of the pipe, namely the point r/R = 0.0. This condition is considered in viscid flow so that the friction effect is very small, almost non-existent.

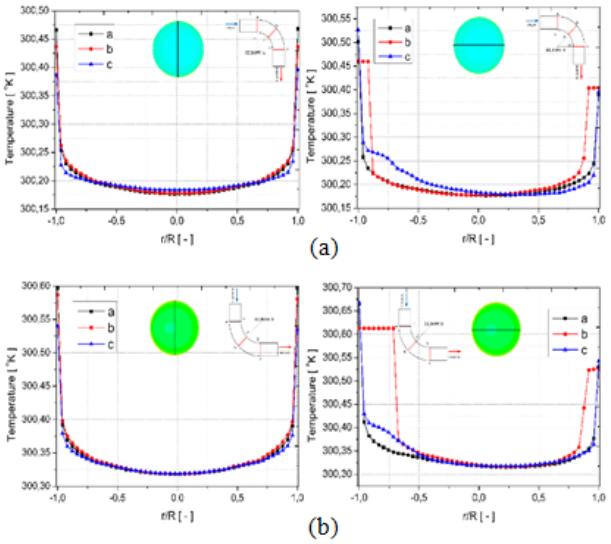

Figure 11: Temperature distribution at Re = 350.551for (a) Elbow A and (b) Elbow B

IV. CONCLUSION

From the results of this simulation, several important results were found which are summarized as follows: The secondary flow is formed very strongly at an angle of 45^{o} for both elbows. The flow velocity reaches a maximum at the same corner location on the inner diameter of the elbow. For pressure losses in the test with Re = 165,748 the flow experienced a pressure loss of 1471 Pa while in the test with Re = 350,551 the flow experienced a pressure loss of 5439 Pa. This shows that an increase in the Reynolds number causes an increase in pressure loss. In addition, an increase in the Reynolds number also causes the friction factor to decrease so that the heat transfer on the wall increases as a result; the flow with a higher Reynolds number has a lower temperature.

REFERENCES

[1] Arvanitis, K.D., Bouris, D. and Papanicolaou, E. 2018. Laminar flow and heat transfer in U-bends: The effect of secondary flows in ducts with partial and full curvature. *International Journal of Thermal Sciences*. 130, February (2018), 70–93.

[2] Ayala, M. and Cimbala, J.M. 2021. Numerical approach for prediction of turbulent flow resistance coefficient of 90° pipe bends. *Proceedings of the Institution of Mechanical Engineers, Part E: Journal of Process*

ISSN (online): 2581-3048
Volume 7, Issue 5, pp 154-159, May-2023
https://doi.org/10.47001/IRJIET/2023.705017

Mechanical Engineering. 235, 2 (2021), 351–360.

[3] Banakermani, M.R., Naderan, H. and Saffar-Avval, M. 2018. An investigation of erosion prediction for 15° to 90° elbows by numerical simulation of gas-solid flow. *Powder Technology*. 334, (2018), 9–26.

[4] Ikarashi, Y., Uno, T., Yamagata, T. and Fujisawa, N. 2018. Influence of elbow curvature on flow and turbulence structure through a 90° elbow. *Nuclear Engineering and Design*. 339, September (2018), 181–193.

[5] Ji, Y. and Liu, S. 2019. Effect of secondary flow on gas-solid flow regimes in lifting elbows. *Powder Technology*. 352, (2019), 397–412.

[6] Lin, R. 2011. Issues on Clean Diesel Combustion Technology Using Supercritical Fluids : Thermophysical Properties and Thermal Stability of Diesel Fuel. *Biomedical and Chemical Engineering*. (2011), 419.

[7] Nayak, B.B., Chatterjee, D. and Mullick, A.N. 2017. Numerical prediction of flow and heat transfer characteristics of water-fly ash slurry in a 180° return pipe bend. *International Journal of Thermal Sciences*. 113, (2017), 100–115.

[8] Rawat, A., Singh, S.N. and Seshadri, V. 2020. CFD analysis of the performance of elbow-meter with high concentration coal ash slurries. *Flow Measurement and Instrumentation*. 72, May 2019 (2020), 101724.

[9] Rosman, M. and Pao, W. 2017. *Temperature Prediction in Hot Tapping Process for High Pressure Pipeline*.

[10] Sutton, E., Juel, A., Kowalski, A. and Fonte, C.P. 2022. Dynamics and friction losses of the flow of yield-stress fluids through 90° pipe bends. *Chemical Engineering Science*. 251, (2022), 117484.

[11] Tan, Y., Zhang, H., Yang, D., Jiang, S., Song, J. and Sheng, Y. 2012. Numerical simulation of concrete pumping process and investigation of wear mechanism of the piping wall. *Tribology International*. 46, 1 (2012), 137–144.

Citation of this Article:

Sefrian Imam B, Khoiri Rozi, Agus Suprihanto, Susilo Adi W, Yunianto Arif S, "Flow Analysis of Pertamina-Dex in Curved Pipe Line at the Integrated Terminal of Pertamina Patra Niaga Semarang" Published in *International Research Journal of Innovations in Engineering and Technology - IRJIET*, Volume 7, Issue 5, pp 154-159, May 2023. https://doi.org/10.47001/IRJIET/2023.705017

****

